Baffin Bay sea ice inflow and outflow:1978/1979-2016/2017

Reviewer 1

General comments:

The revised version of this manuscript is greatly improved. The comments from the previous reviews have been properly addressed. Only minor reviews remain.

Minor revisions:

P1. L.19-20: Change NWP acronym to the one commonly used for the North Water Polynya (NOW). NWP is used for North West Passage in the Arctic.

Response: The 'NWP' has been replaced by 'NOW' throughout the manuscript.

P.2 L.10: change "influences on" to "influence"

Response: Changed as suggested.

P.3 L.21: change "of necessary" to "necessary".

Response: changed as suggested

P.4 L.3-4: I would change this sentence to say that this study focuses on the period of November 1978 to February 2017. No need to say that this was the data available at the time of the study.

Response: We reconstruct the sentence without emphasizing that the study period is in line with data time period available.

P.9 L.17: change "convoluted" to "convolved". This is the proper mathematics term.

Response: changed as suggested

P.17 L.5: Change "There sources" to "The sources that".

Response: changed as suggested

Reviewer 2

General Comments:

The paper has changed significantly and now focuses on sea ice area flux through Baffin Bay, using three gates (different ones compared to the first version). The authors also expand the time series, now including the full time span of the NSIDC ice motion data set starting in 1978. The comparison with the Fram Strait flux has been discarded.

Unfortunately, the revision does not include a track of the changes in the new version of the paper. But from what I found, it seems that major parts of the paper have been rewritten and restructured. This is acknowledged and I find the paper improved now, following a certain thread. Also the quality and compilation of figures has improved.

Response: Thanks a lot for the supporting comments above.

The major objective of the paper is to derive long term trends and variations in sea ice flux through Baffin Bay. Former studies (Cuny et al., 2005, Curry et al., 2014, Kwok, 2007) have presented sea ice flux retrievals in the Baffin Bay already, but only on shorter time scales. Still, my major objections are regarding the soundness of the study:

1. Evaluation of the sea ice motion: The authors write: "To assess the NSIDC data, a reference product of sea ice motion, which is visually retrieved from high-resolution (~100 m) Envisat

wide-swath (~450 km) observations, is employed". I wonder what is meant by "visually"? It should be based on a robust retrieval algorithm!? In any case, you should describe how you have retrieved the reference ice drift from the Envisat data in much more detail. Moreover, it is not well described how the comparison is performed.

Response: It's our mistake not showing the method that we adopted. Indeed, the SAR-derived sea ice motion product is obtained following the algorithm provided in Kowk et al. (1990) to track common feature on images in sequence. In the revised manuscript, we present the information about this. Additional knowledge to sort out the erroneous Envisat-derived sea ice drifts are also given. That is, ice motion with a speed of larger than 5% of the NCEP wind is discarded, since they are likely related to the tracking of weather features. Visually inspect is finally used to identify the possible remaining small portion of erroneous ice motion that are not excluded by the 'wind' rule. Then, if the sea ice speed or direction value of a grid lying out of mean $\pm$2standard deviation of those of the surrounding eight grids in a 3×3 matrix, it is treated as an invalid estimate. Inverse distance interpolation is used to give an estimate for grids without valid ice motion estimates. Please see the second paragraph in revised texts in P4. Moreover, more details about how to compare the two products are also shown. Please see the third paragraph in revised texts in P4 (i.e., between line 7 and line 16).

2. For the uncertainty of the NSIDC ice motion, you use the standard deviation of difference (3.11 km/day) between the NSIDC and Envisat-derived ice drift. I don't think that this accounts for the real uncertainty. There is a nice paper by Sumata et al. (2015), which provides an empirical error function for different sea ice drift products, including the NSIDC retrieval. It also shows that the uncertainty increases with higher drift speeds, i.e. underestimation of high drift speeds.

Response: Thanks very much for showing us study by Sumata et al (2015). In the revision, we adopted the empirical uncertainty function as given in Sumata et al. (2015) to estimate the NSIDC ice motion uncertainty, which is in related to sea ice concentration and drift speed variations. The uncertainty are recalculated and updated estimates are shown in Table 1. As suggested, this consideration helps to avoid the likely underestimation of uncertainty with respect to the high drift speed fields.

3. The study heavily relies on the NSIDC data set and assumes that this data set is consistent over the entire period from 1978-2018, despite the fact that many different sensors have been used for different periods to construct this time series. In order to calculate trends, the consistency should be validated and profound uncertainty estimates have to be provided.

Response: To verify the consistency of NSIDC ice motion for the periods before and after 1987, we compare the NSIDC data of the two periods to corresponding IABP buoy measurements. As shown in Figure 2, the bias and standard deviation of difference between NSIDC and IABP data are similar over the 1979-1987 (Figure 2a) and 1988-1994 (Figure 2b) periods. The agreement indicates that there is no significant difference for NSIDC ice motion data in the earlier 1979-1987 and latter periods.

4. The ice growth model used in section 2.3 is very basic and simple. For example, it does not handle variations in the snow cover?! Moreover, the derived decrease in thickness is then used to explain trends in the ice motion due to wind (see Eq 2). But the air-ice drag coefficient is not considered here neither, although it is an important parameter, resulting from the surface and bottom roughness of the sea ice. This approach seems to be very vague.

Response: We sincerely appreciate this insightful suggestion. IceBridge measurements point to that a declining trend exists in snow depth over first-year ice cover in Arctic Ocean, suggesting the potential impacts on ice thickness growth rate and thus long-term sea ice thickness changes. Therefore, using the simple ice growth model to estimate sea ice thickness changes, by only taking into account the decreased freezing day degrees while neglecting the impacts owing to snow depth changes, may overestimate the declining trend of sea ice thickness. However, the relative consistency of increases in ice motion speed as derived from NSIDC data and our calculations using Eq.3 demonstrates that our estimates are credible (For more information, please see the last paragraph in Section 5.3.2). In the revised manuscript, we notice the readers to pay attention to this limitation when understanding our results.

Yes, variations of drag coefficient can influence the sea ice drift rate. A recent study indicates that air-ice and water-ice drag coefficients in Baffin Bay show increasing trends, by the order of approximately 0.01×10^{-3}/yr and 0.06×10^{-3}/yr, respectively (Tsamados et al., 2014). Considering this, we reassess the increase of sea ice motion due to the changes in air and water drag coefficients. The new estimates indicate that both sea ice thickness decrease and drag coefficients increases contribute a significant part to the sea ice motion increase in Baffin Bay area. (For more information, please see the last paragraph but one in Section 5.3.2).

Detailed comments:

P2L5: "a northward flowing West Greenland Current (WGC) along the Greenland coast 5 carries warm and salty water from the North Atlantic" … Figure 1 says it is "cold"?

Response: It's a mistake in Figure 1and We removed it.

P4L5-16: How is the reference ice drift derived?

Response: We present the used algorithm as provided in Kowk (1990). Moreover, to sort out erroneous drift, we use NCEP reanalysis wind as a reference. That is, sea ice motion that are larger than 5% of wind are sored out, since they are likely related the tracking of weather features. See P4 Line 7-11.

Figure2: Are you comparing different periods? It looks like you compare Envisat ice drift from Feb 19-22 with NSIDC ice drift from Feb 4-7. You have to describe in much more detail how the comparison between NSIDC and Envisat ice drift is performed and how Envisat ice drift is derived.

Response: Figure 2 is modified. The derived sea ice drift in Feb 4-7 and 19-22 are separately presented, together with the NSIDC data in the corresponding periods. Please see Figure 3 in the revised manuscript.

Figure 4: Fast ice edges from the different periods are hard to distinguish. May be zoom in the different regions.

Response: Figure 4 is modified (see Figure 5 in the revised paper). Key regions with fast ice extent variations are enlarged to distinguish the fast ice extent variations during different months.

Section 2.2.2: The used gates in other studies seem to be at different locations. How does this affect the comparison?

Response: To investigate the estimates due to the difference locations of the gate, we derived the area flux through a gate further south as used in the previous studies near to the Davis Strait. Although the previously-used gate is narrower compared to the south gate used in this study, we found the faster ice drift compensate the difference in the sea ice area flux due to the flux width changes. Indeed, the area flux in the south gate (this study) and the Davis Strait gate (previous study) is in good agreement (not shown).

Figure 10: How do you explain that the mean sea ice area flux in the 1978-1987 period is so low compared to the later periods? In any case, this needs to be investigated in more detail (see my concern

about the consistency of the NSIDC data set).

Response: We compare the NSIDC data to IABP buoy measurements with data for the 1979-1987 and 1988-1994 periods. For more details, please see Figure 2 in the revised manuscript. Uncertainty scales (bias and standard deviation of the two ice speed difference) do not show remarkable difference over the earlier (1979-1987) and the later (1988-1994) periods.

Figure 12: unit - How do you derive “km” from the divergence of a velocity field? Should it not be 1/s (or 1/d) ?

Response: Corrected as suggested. (See Figure 13 in the revision).

Baffin Bay sea ice inflow and outflow:1978/1979-2016/2017

Haibo Bi[1,2,3], Zehua Zhang[1,2,3], Yunhe Wang[1,2,4], Xiuli Xu[1,2,3], Yu Liang[1,2,4], Jue Huang[5], Yilin Liu[5], Min Fu[6]~~Haijun Huang[1,2,3,4]~~

带格式的：字体：小四，上标

[1]Key laboratory of Marine Geology and Environment, Institute of Oceanology, Chinese Academy of Sciences, Qingdao, China

[2]Laboratory for Marine Geology, Qingdao National Laboratory for Marine Science and Technology, Qingdao, China

[3]Center for Ocean Mega-Science, Chinese Academy of Sciences, Qingdao, China

[4]University of Chinese Academy of Sciences, Beijing, China

[5]Shandong University of Science and Technology, Qingdao, China

[6]Key Laboratory of Research on Marine Hazard Forecasting Center, National Marine Environmental Forecasting Center, Beijing, China

带格式的：上标

Correspondence to: ~~Haijun Huang~~Haibo Bi (~~hjhuang~~bhb@qdio.ac.cn)

Abstract.

Baffin Bay serves as a huge reservoir of sea ice which would provide the solid fresh water sources to the seas downstream. Employing satellite-derived sea ice motion and concentration fields, we obtain a nearly 40-yr record (1978/1979-2016/2017) of the sea ice area flux through key fluxgates of Baffin Bay. Based on the estimates, Baffin Bay sea ice area budget in terms of inflow and outflow are quantified and possible causes for its interannual variations and trends are analyzed. On average, the annual (September-August) inflows through the North Gate and Lancaster Sound are on the order of 205.8(±74.7)$\times10^3$km^2 and 55.2(±17.8)$\times10^3$km^2, respectively. In particular, a comparison with published results seem to suggest that about 75%~85% of the inflow through the North Gates is newly-formed ice produced in the recurring North Water Polynya (~~NWP~~NOW), in addition to the inflow via Nares Strait and Jones Sound. Meanwhile, the mean outflow via the South Gate approaches to 394.3(±110.2)$\times10^3$km^2. The distinct interannual variability for ice area flux through the North Gate and South Gate is partly explained by wind forcing associated with cross-gate sea level pressure difference, with a correlation of 0.62 and 0.68, respectively. Also, significant increasing trends are found for the annual sea ice area flux through the three gates, amounting to 38.9$\times10^3$km^2/de, 82.2$\times10^3$km^2/de, and 7.5$\times10^3$km^2/de for the North Gate, South Gate, and Lancaster Sound, respectively. These trends are chiefly related to the increasing ice motion which is associated with a thinner ice owing to the warmer climate (i.e. higher surface air temperature and shortened freezing period) and increased air and water drag coefficients over the past decades~~ (i.e. higher surface air temperature and shortened freezing period)~~.

1. Introduction

Baffin Bay is a semi-enclosed ocean basin that connects the Arctic Ocean and the Northwest Atlantic (Figure 1). It covers an area of 630 km^2 and is bordered by Greenland to the east, Baffin Island to the west, and Ellesmere Island to the north. From the north to the south, the bay spans approximately 1280 km. In the north, it connects the Arctic Ocean through Nares Straits and the channels of the Canadian Arctic Archipelago (CAA). In the south, the bay is separated from the Labrador Sea by Davis Strait (~350 km in width). The width of the bay varies greatly, with a range of approximately 100 km to 600 km.

The mean circulation of Baffin Bay is characterized by a cyclonic pattern (Figure 1) (Melling et al., 2001; Dunlap and Tang, 2006). In the east side of the bay, a northward flowing West Greenland Current (WGC) along the Greenland coast carries warm and salty water from the North Atlantic. On the west side, the Baffin Current (BC) flows southward along the coast of Ellesmere and Baffin Island, bringing cold and fresh Arctic water and sea ice through Baffin Bay to Labrador Sea. Therefore, Baffin Bay serves as an important sea ice reservoir and is an important fresh water source to Labrador Sea downstream (Curry et al., 2014; Qian et al., 2016; Cuny et al., 2002). A direct potential consequence of sea ice outflow is the formation of lighter sea-water that will strengthen the stratification of Labrador Sea through stabilizing the water column (Goosse et al., 1997; Rudels, 2010; Curry et al., 2014; Qian et al., 2016). These changes will potentially influence~~s on~~ the strength of the meridional overturning circulation mechanism of the North Atlantic Ocean which ultimately affects global deep-water circulation and exchanges (Aagaard and Carmack, 1989; Holland et al., 2001; Jahn et al., 2010; Hawkins et al., 2011; Cimatoribus et al., 2012; Yang et al., 2016).

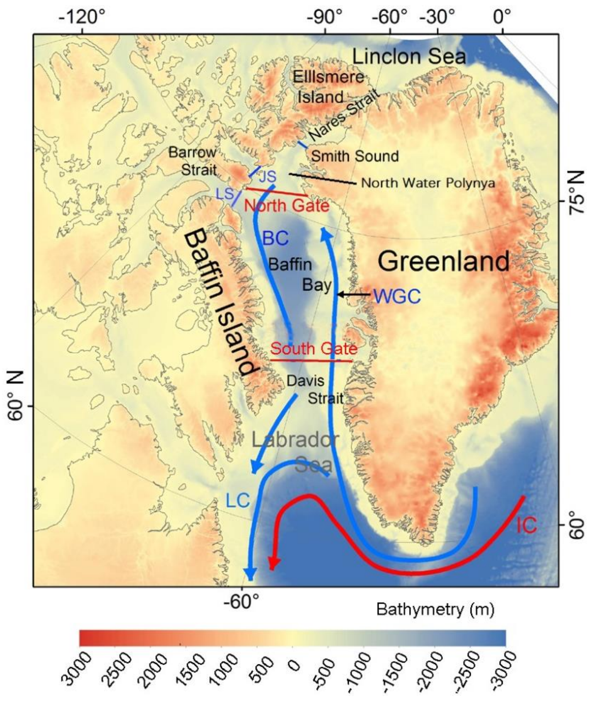

Figure 1. The mean circulation pattern in Baffin Bay (blue and red arrows) and the locations of the key fluxgates to assess sea ice area flux through the bay. The ~~colder ~~west Greenland current (WGC), Baffin Current (BC), and Labrador Current (LC) are marked with blue arrows. The ~~warmer ~~Irminger Current (IC) is represented by the red arrow. The key fluxgates through which sea ice floats into the bay includes Nares Strait, Jones Sound (JS), and Lancaster Sound (LS). Area flux

through a defined North Gate together with the LS flux is used to quantify the sea ice area inflow to the bay. The outflow fields are depicted using flux via the South Gate.

Sea ice inflow and outflow have been considered as important variables for interpreting the sea ice area balance of the Arctic Ocean (Kwok et al., 2005; Spreen et al., 2006; Kwok, 2007; Kwok, 2009; Kwok et al., 2010; Smedsrud et al., 2011; Krumpen et al., 2013; Kwok et al., 2013; Bi et al., 2016a; Bi et al., 2016b; Krumpen et al., 2016; Smedsrud et al., 2017; Zhang et al., 2017). For instance, satellite-derived sea ice export has been investigated in some key water fluxgates around the periphery of the Arctic Basin, with Fram Strait being the primary focus of study owing to its significant contribution to the changes of the Arctic sea ice extent (Smedsrud et al., 2011; Smedsrud et al., 2017). In Baffin Bay, sea ice loss due to outflow through Davis Strait can be largely replenished by the inflows from the north though the Lancaster Sound (LS), Jones Sound (JS), and Nares Strait (Figure 1). Additionally, North Water Polynya (~~NWP~~NOW), approximately located between Smith Sound and the North Gate (Figure 1 and S1), is deemed as an important source of newly-formed sea ice to the bay.

带格式的: 缩进: 左 0 字符, 首行缩进: 1.5 字符

Baffin Bay sea ice inflow and outflow have significant implications for understanding the current radical climate change, becasue a strong atmospheric warming trend has been widely noted in the northern high latitudes (Serreze et al., 2009; Stroeve et al., 2014; Graham et al., 2017; Stroeve et al., 2018). In Baffin Bay, surface air temperature has increased by 2 to 3 ℃/de since the late 1990s (Peterson and Pettipas, 2013), resulting in prolonged days of sea ice melting there (i.e. earlier melting onset and delayed ice-freezing startup) (Stroeve et al., 2014). Accordingly, a rapid decline of sea ice coverage in all seasons has been clearly identified in the bay (Comiso et al., 2017b; Parkinson and Cavalieri, 2017). Within the context of such a pronounced climate change, examining the variability and trends in sea ice outflow through Baffin Bay over a long time series is of particular interest. Although interannual variability in sea ice inflow and/or outflow components in Baffin Bay has been reported in several studies (Cuny et al., 2005; Kwok, 2007; Curry et al., 2014), robust knowledge of their trends is ~~of~~ necessary to predict future changes and validate model results. This study attempts to provide an extended record of the satellite-derived sea ice inflow and outflow over nearly four decades (1978/1979-20116/2017) through the key fluxgates of Baffin Bay and to examine the possible causes of the trends.

2. Data description

2.1 Data

2.1.1 Sea ice motion

The Polar Pathfinder Daily 25 km EASE-Grid Sea Ice Motion Vectors product was provided by the National Snow and Ice Data Center (NSIDC) (Tschudi et al., 2016). This product has been widely used by the modeling and data assimilation communities (http://nsidc.org/data/NSIDC-0116). It is derived from a variety of sensors on satellite platforms, including the

Advanced Very High Resolution Radiometer (AVHRR), Scanning Multichannel Microwave Radiometer (SMMR), Special Sensor Microwave Imager (SSM/I), Special Sensor Microwave Imager Sounder (SSMIS), and Advanced Microwave Scanning Radiometer-Earth Observing System (AMSR-E), and merged with buoy measurements from the International Arctic Buoy Program (IABP) to obtained estimates determined from the reanalyzed wind data. ~~When conducting the present study this product was available for~~This study focuses on the period from November 1978 to February 2017 (Tschudi et al., 2016).

To assess the NSIDC data, a reference product of sea ice motion, which is ~~visually~~ retrieved from high-resolution (~100 m) Envisat wide-swath (~450 km) SAR observations following methods in Kwok et al.(1990) that tracks the common ice features on image in sequence, is employed. Sea ice motion is mostly 0~1% of the wind in the Arctic Ocean (Thorndike and Colony, 1982). Therefore, sea ice motion that is larger than 5% of wind (NCEP reanalysis surface wind) are sored out, since it is likely related the tracking of weather features. Visually inspect is further conducted to identify the possible remaining erroneous ice motion fields that are not discriminated by the 'wind' rule. Then, if the sea ice speed or direction value of a grid lying out of mean ±2standard deviation of those of the surrounding eight grids in a 3×3 matrix, it is treated as an invalid estimate. The inverse distance interpolation method is then used to give an valid estimate for the grid.

The Envisat estimates, sampled on a 10 km grid cell, have an overall uncertainty of ~300 m (Kwok, 2007). To facilitate a direct comparison, the spatial resolution of the ~~final~~ derived Envisat estimates are ~~smoothed~~ degraded to a 25-km grid~~, and then spatially registered to~~ consistent with the NSIDC ~~data~~grids. NSIDC sea ice motion and SAR ice motion vectors in terms of drift speed (U_{NSIDC}, U_{SAR}, in unit of km/d) and angle (or direction) are obtained at a given location and compared. The quality of the NSIDC is examined by the following scale: sea ice speed bias (U_{NSIDC}-U_{SAR}) (Figure 3a) and angular (directional) difference of the sea ice drift vector (Figure 3b). Furthermore, IABP buoy measurements of daily mean sea ice motion from January 1979 to December 1994 (http://iabp.apl.washington.edu/) are used to assess the consistency of NSIDC-based sea ice area flux between the 1978-1987 and the later periods. There is at least 10 buoys in operation during 1979-1994 period in the Arctic Ocean. Overall comparisons in Figure 2 suggest that no significant difference with respect to the U_{NSIDC}-U_{SAR} fields at different speed ranges is found between the two periods: 1979-1987 (Figure 2a) and 1988-1994 (Figure 2b).

带格式的：字体：倾斜

带格式的：下标

带格式的：字体：倾斜

带格式的：下标

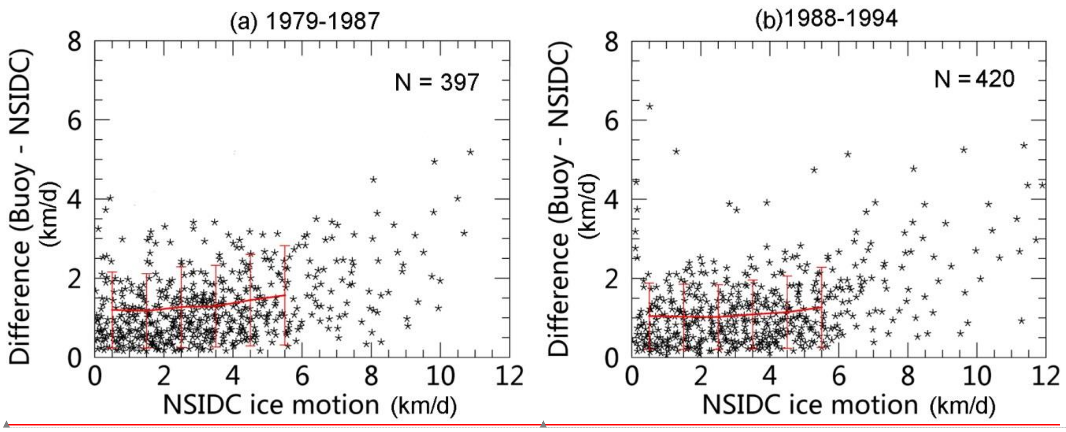

Figure 2. Sea ice motion difference between IABP and NSIDC products at different ice drift speeds during (a) 1979-1987 and (b) 1988-1994 periods. The mean (red line) and standard deviation (error bar) of the difference at different speed ranges (from 0~6 km/d with a bin interval of 1 km/d) are shown. N is the data pair number in comparison.

Two examples of Envisat ice motion fields, acquired on February 2007, are shown in Figure ~~2~~3. One example covers a cyclonic circulation along the west coast of Greenland (~~red~~ blue arrow, Figure 3a) and the other is located in the area next to Davis Strait (blue arrow, Figure 3b). Overall, ~~Comparative~~ comparative results (Figure ~~3a~~4a) present a mean bias of -0.68 km/day in ice speed between the two records (i.e., slightly slower NSIDC) but a relatively large standard deviation of difference (3.11 km/day). Furthermore, there is a small average difference of 3.4 ° in vector angle (Figure ~~3b~~4b), indicating that the NSIDC motion is likely biased to the right. A large standard deviation exists in the difference of motion vector angle (38 °), which is mostly caused by data pairs for the slower Envisat motions of less than 3 km/day (Figure ~~3b~~4b). Despite these phenomena, the two estimates agree well as a whole, as indicated by the high correlation between them (R = 0.87).

带格式的：字体颜色：文字 1

带格式的：缩进：首行缩进： 0 字符

带格式的：字体颜色：文字 1

带格式的：字体：非加粗

带格式的：字体：非加粗

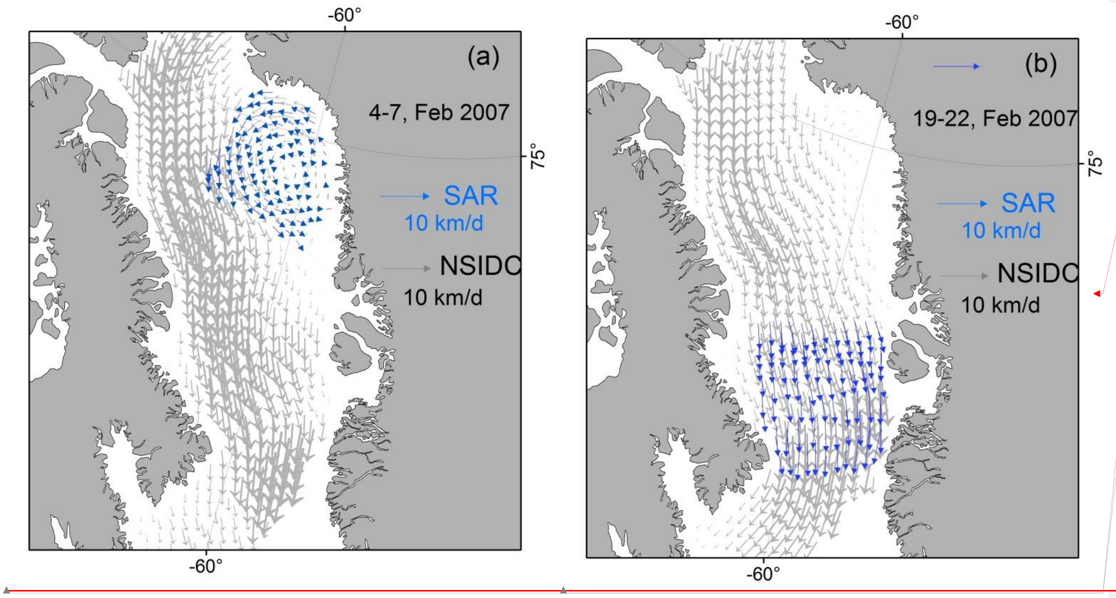

Figure ~~2~~3. Sea ice motion examples from NSIDC and Envisat. Gray arrows corresponds to the NSIDC data ~~on 4~7 February 2007~~. The superimposed blue arrows, one for 4~7 February 2007 (~~red~~a) and the other for 19~22 February 2007 (~~blue~~b), denote the ~~smoothed~~ corresponding Envisat estimates.

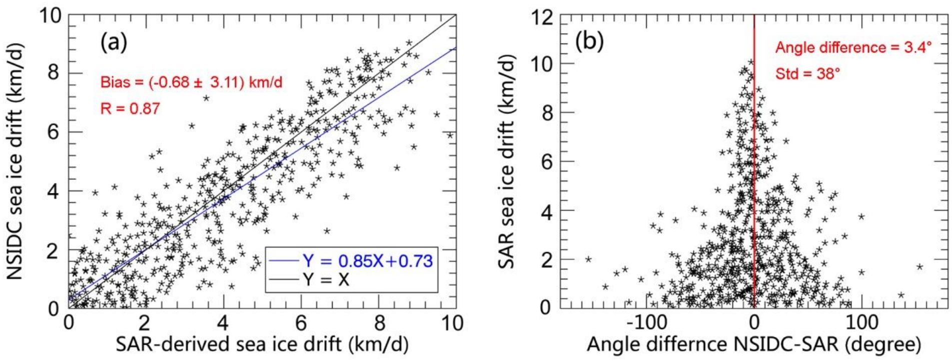

Figure ~~3~~4. Comparison between NSIDC ice motion and Envisat SAR estimates in terms of (a) drifting speed and (b) angular direction.

2.1.2 Sea ice concentration

Satellite-derived daily sea ice concentration records (1978-2017) were obtained from NSIDC (http://nsidc.org/data/NSIDC-0079). These data are derived from the passive microwave observations from SMMR onboard the Nimbus-7, the SSM/I onboard the Defense Meteorological Satellite Program (DMSP) -F8, F11 and F13, and SSMIS aboard DMSP-F17 by the application of Bootstrap algorithm (Comiso et al., 2017a). For the period November 1978 to July

带格式的：字体颜色：文字 1

带格式的：两端对齐，右 -1.57 字符

带格式的：字体颜色：文字 1

1987 the ice concentration is available every other day. The data gap is filled using a temporal interpolation from the data of the two adjacent days (i.e. the previous and subsequent days). The concentration field utilized here is an up-to-date version (v3.1), offering improved consistency among the estimates from the different sensors through the use of daily varying tie points. Furthermore, the product has been optimized to provide enhanced removal of weather and land contaminations (Cho et al., 1996). The data are available with an equal-area grid cell structure (25 km×25 km) on a polar stereographic projection.

2.1.3 Sea ice map of the Canadian Ice Service

Weekly sea ice maps were provided by the Canadian Ice Service (CIS). As shown in Figure S1, sea ice classification and concentration in Baffin Bay are depicted in details on the CIS map. The CIS ice map benefits this study in the following three aspects. First, it is useful for identifying sea ice location and coverage for the ~~NWP~~NOW. Second, it enables the separation of fast ice from floating sea ice. The retrieved CIS fast ice extents are useful for detecting those coastal grid cells where ice motion should be set to zero before the calculation of sea ice area flux. As shown in Figure ~~4~~5, the eastern and western endpoint grids of the North and South Gates, which is possibly covered by fast ice, is expected to have zero motion (see the zoomed regions marked as A, B, and C in Figure 5). This verification serves to reduce possible systematic errors in the estimation of total area flux. In addition, the fast ice extent identified from CIS can be used to interpret the slower ice motions adjacent to the west coast of Greenland (around 75 °N, Figures ~~2~~3). Third, the CIS map facilitates the identification of ice bridges (or ice arches) which typically form in Nares Strait (Figure S1). The formation of ice bridge is a common scenario during the cold freezing period in the strait and the CAA channels, which can substantially restrain Arctic sea ice inflow into Baffin Bay. Typically, two distinct bridges form: one at the northern entrance of Nares Strait adjacent to Lincon Sea (the north bridge) and one near the southern exit of the strait (the south bridge, Figure S1a). The formation of the south bridge can fully restrict the sea ice inflow into northern Baffin Bay, as indicated by the recurring low-concentration regime just downstream of the south bridge (Figure S1b).

带格式的: 段落间距段后：0 磅

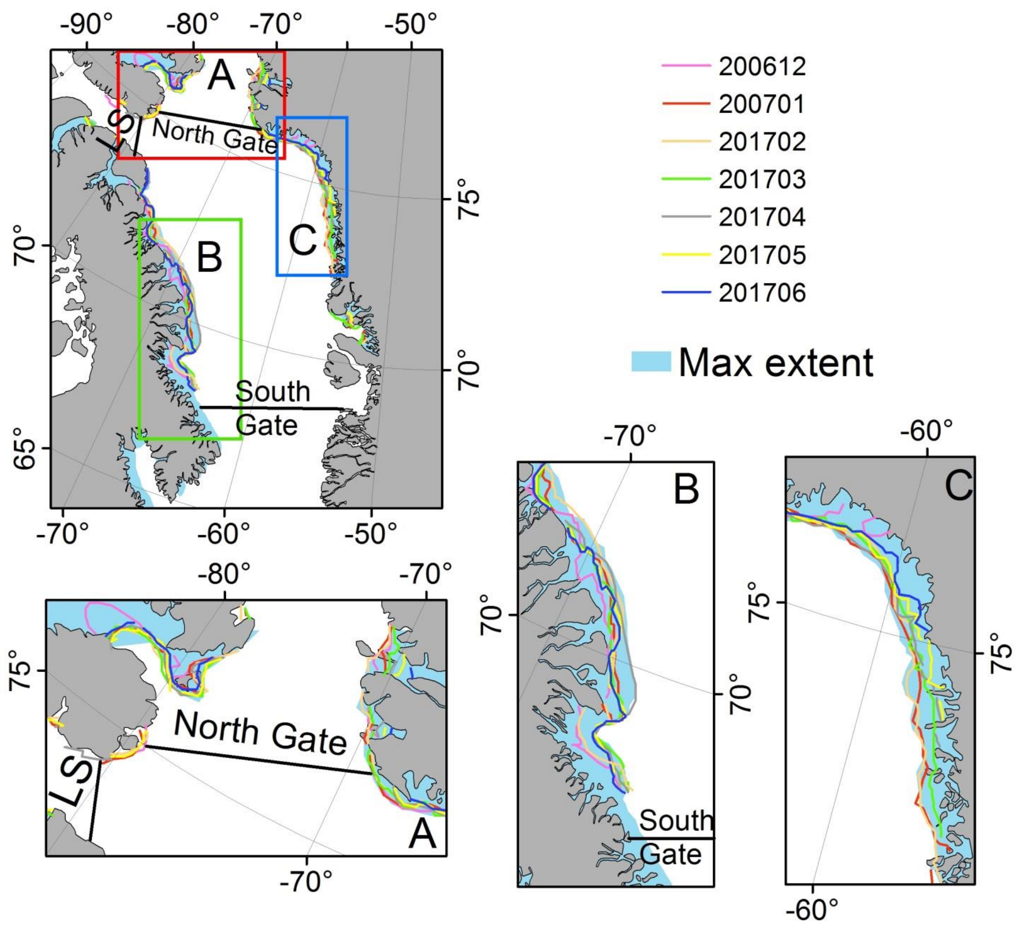

Figure 45. Monthly mean fast ice extent obtained from the CIS map for the period from December 2016 to June 2017. Typical fast ice regions (A, B, and C) in Baffin Bay are zoomed to distinguish the fast ice extent during different periods. The fluxgates are also presented.

2.1.4 Reanalysis data

The reanalysis data of sea level pressure (SLP) and surface air temperature (SAT), used to analyze the impacts of climate changes on ice area flux, were provided by the National Centers for Environmental Prediction/National Center for Atmospheric Research (NCEP/NCAR) (Kalnay et al., 1996). The data are available with a spatial resolution of 2.5 °×2.5 °.

2.2 Sea ice area flux estimation

2.2.1 Methods to estimate sea ice area flux and its uncertainty

Sea ice area flux is estimated by taking the integral of the product between the gate-perpendicular component of the sea ice motion and concentration across one fluxgate (Kwok, 2007). The area fluxes through the North Gate and the Lancaster

带格式的：字体颜色：文字 1

带格式的：两端对齐

Sound (Figure 1) are deemed as the two sea ice inflow components for Baffin Bay. The North Gate (Figure 1), spanning ~320 km in width, is positioned at ~75 °N between 79 °W and 68 °W, where sea ice inflow originates from three components: Jones Sound, Nares Strait, and ice produced from the ~~NWP~~NOW. Another important source of sea ice inflow is Lancaster Sound, which has a gate width of ~80 km and can be computed with the 25-km NSIDC sea ice fields. In contrast, reliable estimates of sea ice area flux for Jones Sound and Smith Sound are not practical due to their small widths (~40 km) with respect to the 25-km pixel resolution of the NSIDC data. Therefore, the results of several studies of the two gates are used to analyze the possible ice inflow contributions to northern Baffin Bay (see Section 5.1 for more details). For the outflow component, sea ice area flux across the South Gate is estimated. The gate spans ~480 km and is located at ~68 °N between 63 °W and 53 °W, close to Davis Strait (Figures 1 and ~~4~~5).

Before computing the area flux, the NSIDC ice motion is first interpolated to a gate to retrieve the gate-perpendicular component of ice motion. Sea ice concentration is used to weight the influences of the open water fractions on the area flux estimates. Following the trapezoidal rule, sea ice area flux (F) integrated across a fluxgate is derived as,

$$F = G\sum_{i=1}^{N-1} u_i c_i (i = 1,2,\dots,N) \qquad (1)$$

where N is the number of along-gate grids. G corresponds to the width of a grid cell (25 km), u_i is the perpendicular component of the sea ice motion, and c_i is the sea ice concentration at the i-th grid cell. As mentioned above, prior to the calculation, the sea ice motion fields at the endpoints of the fluxgate should be set to zero if they are covered by fast ice as recognized in the CIS maps.

The monthly sea ice area flux is calculated as the cumulative daily flux over a calendar month. Similarly, the annual flux denotes the sum of the monthly area flux of one year (September-August). The errors in the daily area flux estimate can be calculated as follows (Kwok, 2009): $\sigma_D = \sigma_u L/\sqrt{N_S}$, where L is the width of the defined gate, σ_u is the uncertainty in daily motion and N_s is the number of independent grid cells across the gate (Table 1). For σ_u, –we use the derived empirical error functions of mean Arctic sea-ice drift (Sumata et al., 2015). The uncertainty function is associated with sea ice concentration and speed variations, and varies in different seasons. ~~we use the uncertainty (3.11 km/day) determined as described above through comparisons with the Envisat ice motion estimates.~~ The uncertainty of monthly area flux is calculated as $\sigma_m = \sigma_D\sqrt{N_D}$, where N_D is the number of days over the month of interest. The annual flux uncertainty is calculated as $\sigma_a = \sigma_m\sqrt{N_m}$, where N_m = 12, i.e., is the number of calendar months from September to the following August, representing a complete seasonal cycle of sea ice growth and decay. The mean uncertainties for different temporal intervals are summarized in Table 1. On average, the annual uncertainties for the North Gate, the South Gate, and LS correspond to small proportions (~~2.5~~3.0%, 2.~~0~~5%, and 2.~~4~~6%, respectively) of the corresponding annual mean flux estimates (provided in Section 4).

Table 1. Mean uncertainty estimates for sea ice area flux in terms of daily (σ_D), monthly (σ_m), and annual (σ_a) fields for the period of 1978/1979-2016/2017. N_s is the number of grid cells covered by the corresponding gate.

Passages	Width (km)	N_s	σ_m (10^3 km^2)	σ_a (10^3 km^2)
North Gate	320	13	1.~~51~~78	~~5.2~~6.17
South Gate	480	19	2.~~27~~81	~~7.86~~9.73
LS	80	3	0.~~38~~41	1.~~31~~42

2.2.2 Comparisons with published results

Based on SSM/I estimates of sea ice motion, Cuny et al. (2005) obtained the sea ice area flux from November through May across Davis Strait over the period 1991/1992-1999/2000 (Figure ~~2~~6, cyan line). During that period, sea ice area outflow was estimated to be 496×10^3 km^2. By comparison, our NSIDC-derived flux through the South Gate (close to Davis Strait) for the same winter months of the same period is on average approximately 380×10^3 km^2. This large difference can be mainly attributed to the distinct contrast in spatial resolution between the two sea ice motion datasets (~70 km for the SSM/I motion data based on 37 GHz observations versus 25-km pixels for the NSIDC data), since larger uncertainty is expected in flux estimates based on a spatially coarser motion. The expected uncertainty in monthly flux based on SSM/I observations was computed as 6.52×10^3 km^2, whereas the uncertainty based on NSIDC motion is 2.27×10^3 km^2 (Table 1). However, the similarity of interannual behavior between the two sets of records is relatively high (R=0.56).

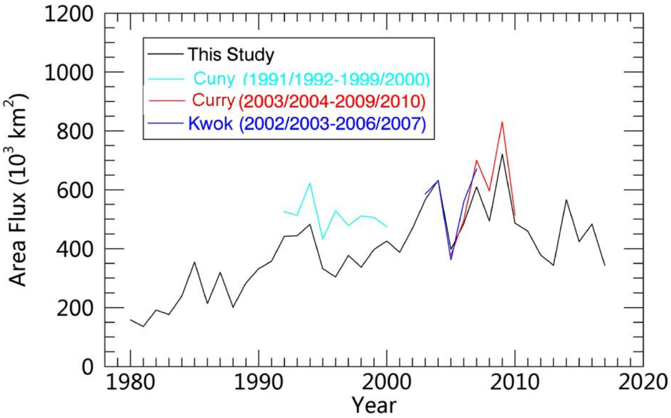

Figure ~~5~~6. Comparison of sea ice area flux (November to the following May) with estimates from Cuny et al. (2005), Curry et al. (2014), and Kwok (2007)

Kwok (2007) used AMSR-E data to examine sea ice drift and export in Baffin Bay over the period 2002/2003-2006/2007 (Figure 6, blue). These estimates were extended to 2009/2010 in Curry et al. (2014) (Figure 6, red). On average, our estimate of the sum of ice area flux for the November-to-May period through the South Gate is -24.3 (±63.7) $\times10^3$ km^2 lower than that provided by Kwok, and -45.5 (±61.0) $\times10^3$ km^2 lower than Curry's estimate (Figure 5). Quantities after "±" are the standard deviation of the difference. Possibly, the differences are primarily caused by the differences in data inputs and slightly due to the small differences in the locations of the defined gates among the different studies. In percentages, the biases are rather small, corresponding to small proportions (4.5% and 8.9%) of the average winter (November~~—~~-May) estimate based on NSIDC data (511×10^3 km^2) for the time range between 2002/2003 and 2009/2010. Moreover, good agreement between the interannual variations of the NSIDC-based results and the AMSR-E-based estimates is identified (Figure ~~5~~6). There is a high correlation of 0.93 between the NSIDC results and the AMSR-E estimates provided by Curry et al. (2014). Overall, the good consistency with the higher-resolution AMSR-E estimates suggests the results of this study are credible.

Note that the location of the south gate is slightly different between our and some previous studies (Cuny et al. 2005; Curry et al. 2014) . To investigate the estimates due to the difference locations of the gate, we derived the area flux through a gate further south as used in the previous studies near to the Davis Strait (Cuny et al. 2005; Curry et al. 2014). Although the previously-used gate is narrower compared to the south gate used in this study, we found the faster ice drift there compensates the difference in the sea ice area flux due to the flux width changes. Indeed, the NSIDC-based area flux in the south gate (this study) and the Davis Strait gate (previous study) is quite similar (not shown).

2.3 Methods to simulate ice thickness changes and investigate the impacts on ice motion

Based on the Zubov ice growth model (h^2+5h=8θ, where θ is C_{Fd}-3C_{Md}, where C_{Fd} and C_{Md} are the cumulative degrees of SAT for freezing and melting days, respectively; for the ice growth period, C_{Md} is set to 0), we obtain preliminary estimates of the ice thickness changes in Baffin Bay. The value of C_{Fd} for an ice growth period can be derived from the NCEP/NCAR reanalysis SAT product. To define a freezing day, we follow Stroeve et al. (2014).

Changes in sea ice thickness impact the sea ice motion fields. To assess the ice motion changes when ice thickness is altered, the standard Quadratic drag laws (Equation 2) are used to examine the ice floe acceleration due to wind (τ_a) and current forcing (τ_w) as follows,

$$\boldsymbol{\tau}_{\mathbf{a}} = \frac{\rho_a C_a}{\rho_i h_i}\left|\mathbf{V}_a - \mathbf{V}_{\mathbf{i}}\right|(\mathbf{V}_{\mathbf{a}} - \mathbf{V}_{\mathbf{i}}) \qquad (2)$$
$$\boldsymbol{\tau}_w = \frac{\rho_w C_w}{\rho_i h_i}\left|\mathbf{V}_w - \mathbf{V}_{\mathbf{i}}\right|(\mathbf{V}_w - \mathbf{V}_{\mathbf{i}})$$

where ρ_a is air density, C_a is the air-ice drag coefficient, V_a is the wind velocity vector, ρ_a is the seawater density, C_w is the water-ice drag coefficient, V_w is the surface ocean velocity vector, ρ_i is the sea ice density, and h_i is the ice floe thickness.

2.4 Sea ice divergence approximation

To gain further insight into the sea ice production due to the ice dynamics in Baffin Bay (see section 4.2 for more details), the divergence ($\nabla\cdot\vec{\mathrm{V}}$) of the sea ice motion vector field is calculated. The derivative of the ice motion field in the x and y direction is calculated by use of the Sobel operator. The Sobel operator is ~~convoluted~~ convolved with the x and y components V_x and V_y of the ice motion field to calculate the divergence,

带格式的：两端对齐

$$\nabla \cdot \vec{V} = \frac{1}{8G}\begin{bmatrix} 1 & 0 & -1 \\ 2 & 0 & -2 \\ 1 & 0 & -1 \end{bmatrix} * V_x + \frac{1}{8G}\begin{bmatrix} 1 & 2 & 1 \\ 0 & 0 & 0 \\ -1 & -2 & -1 \end{bmatrix} * V_y \quad (3)$$

where * is the convolution operator. G is grid cell size of 25 km. The Sobel operator smoothes the field perpendicular to the derivation direction.

3. Sea ice conditions in Baffin Bay

3.1 Sea ice coverage

The characteristic features (2016) of annual sea ice coverage of Baffin Bay are shown in Figure ~~6~~7. The bay is generally ice-free between July and October. From November, the coverage advances rapidly from the west to the east and, from the north to the south. It reaches maximum coverage in later winter (March). The retreat westward around the South Gate starts in April. The southerly circulation and the warm WGC are responsible for the lower ice cover in the east of the South Gate (Figure 1). The identifiable low sea ice concentration fields in the northern part during the cold months are associated with the occurrence of ~~NWP~~NOW (such as in April in Figure ~~6~~7).

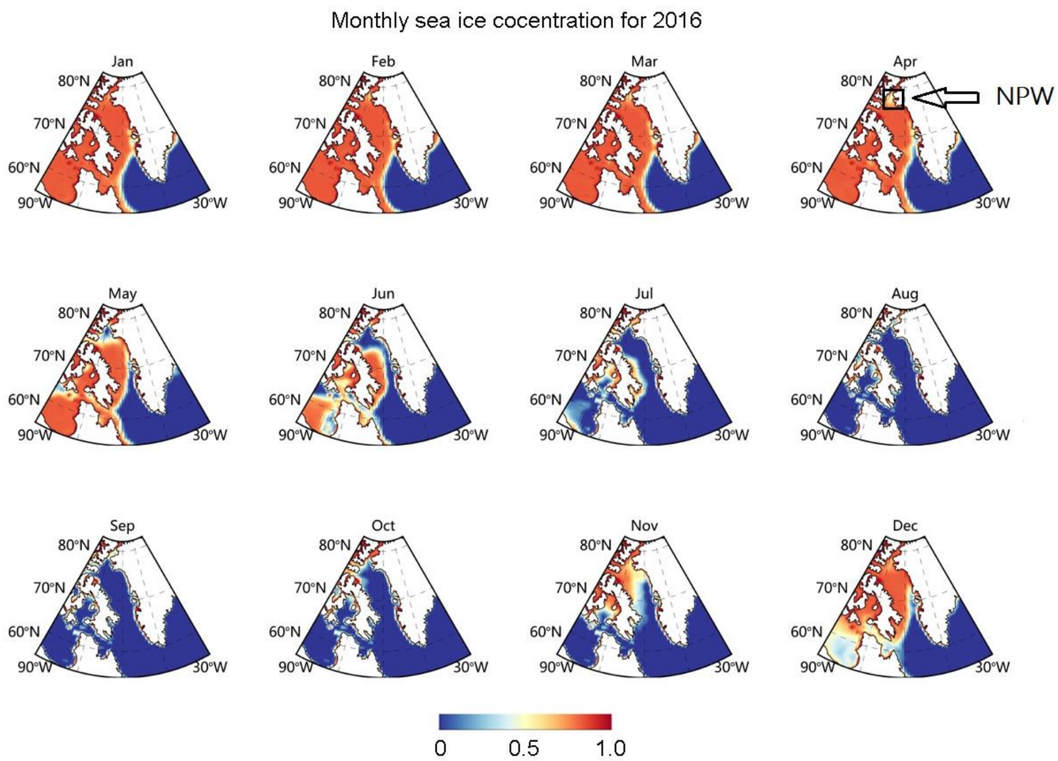

Figure ~~6~~7. Spatial variations of mean sea ice concentration fields for the calendar months in 2016. In the panel for April, ~~NWP~~NOW is outlined.

3.2 Sea ice drift pattern

Two selected examples of sea ice drift in Baffin Bay are shown in Figure ~~7~~8. The March and June cases in 2016 are chosen to represent ice circulation under cold and warm conditions, respectively. Overall, sea ice drift in Baffin Bay is characterized by a cyclonic pattern. To the west, the sea ice motion (Figure ~~7a~~8a) is connected to the northerly Baffin Current (BC, Figure 1). To the east, the slower drift (Figure ~~7a~~8a) and even southerly drift (Figure ~~7b~~ 8b and Figure ~~2~~3), especially in the northeast corner of the bay (around 75 °N), is associated with the southerly West Greenland Current (WGC, Figure 1).

In March, the prevailing drift pattern in the bay is southward (Figure ~~7a~~8a). Sea ice starts from Smith Sound and the south end of Nares Strait and extends southward along the coast of Baffin Island. From the northern end of the bay to Davis Strait, the sea ice motion gradually accelerates, reaching the maximum speeds around Davis Strait (Figure ~~7a~~8a). The mean sea ice speed in the North Gate is 3.2 km/day, whereas sea ice in the South Gate attains a speed of 8.5 km/day. Moreover, the CIS map demonstrates that the thicker multiyear ice from either the Arctic through Nares Strait (Figure ~~S4a~~S1a) or Lancaster Sound (Figure ~~S4b~~S1b) is mostly confined to the west of the bay. In contrast, most of the ice motion fields in June have decreased sharply to less than 0.8 km/day, but the basin-scale cyclonic pattern is still observable (Figure ~~7b~~8b).

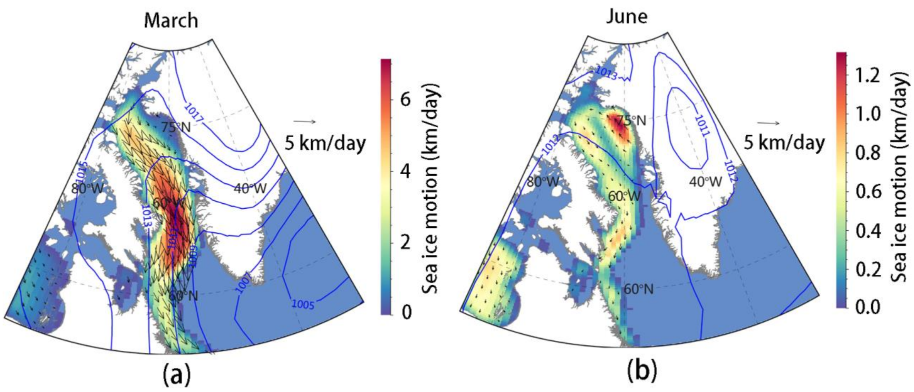

Figure ~~7~~8. Sea ice drift patterns (arrows) in (a) March and (b) June 2016. Background color denotes the magnitudes of sea ice speeds. Superimposed bold curves represent the SLP distribution patterns of the corresponding month.

The general cyclonic sea ice movement pattern can be attributed to the wind forcing associated with the SLP distribution (blue curved lines in Figure ~~7~~8). The associated denser isobars in the bay imply a stronger geostrophic wind flow in March (Figure ~~7a~~8a). The deep SLP trough (as apparent in March, Figure ~~7a~~8a) begins to emerge in October (not shown) and is gradually enhanced until the end of March. The trough enters to a weak stage from April until the end of summer, as evident in June in Figure ~~7b~~8b. The spatial distribution of the trough in June is responsible for the remarkable features of ice circulation, such as the southeasterly flows in the northeast part of the bay and the northwesterly flows in Davis Strait (Figure 7b). Owing to modulation by the structure of the coastline, the actual sea ice drift direction in the bay tends to be on the right of the isobars (Figure ~~7a~~8a).

3.3 Trends in sea ice motion and concentration fields

During cold seasons over the period 1978/79-2016/17, the sea ice concentration fields in Baffin Bay show a basin-scale average declining trend ranging from -1.2%/de (winter, December-February, Figure ~~8a~~9a) to -3.1%/de (spring, March-May, Figure ~~8b~~9b). During the warm seasons (summer: June-August; autumn: September- November), the sea ice decrease is stronger, with an average change rate of -10.4% (not shown). Clear regional variations in the trend fields are apparent in Figure ~~8~~9. Around the southeastern edge during the winter period, sea ice retreats northward and eastward, with a significant decreasing trend in ice concentration, in excess of -10%, relative to the 2.8%/de decline reported earlier along this edge for the period 1951-2001 (Stern and Heide-Jørgensen, 2003). However, sea ice concentration in other regions of the bay shows a quite declining trends weaker than -2.0%/de (Figure ~~8a~~9a).

A small enclosed area of the ~~NWP~~NOW region in the north end of the bay also displays a declining trend in sea ice concentration fields (Figure ~~8a~~ 9a and ~~8b~~9b). In the ~~NWP~~NOW region, there is an average sea ice concentration decrease in winter (-3%/de) and a stronger decrease during spring (-8%/de). This seasonal difference is primarily associated with the appearance of the ice bridge near the Smith Sound in late winter or early spring (February or March). More new ice can be produced from ~~NWP~~NOW during the spring period than the winter, and the recurring ice bridge can largely recede into the ice inflow from the Nares Strait into Baffin Bay. Therefore, higher fractions of the sea ice inflow component originating from ~~NWP~~NOW production seem to occur in spring than in winter. The more recently-produced ice thus contributes to the observed fields of lower concentration in the ~~NWP~~NOW region in spring (Figure ~~8b~~9b). Additionally, the decline in sea ice concentration in the ~~NWP~~NOW seems to be partially associated with the southward sea ice motion (Figure ~~9a~~ 10a and ~~9b~~10b). In the broad regions just south of the ~~NWP~~NOW, the increased southward ice advection provides more chances for the creation of newly-formed ice in polynyas. Therefore, the enhanced southward ice advection through Baffin Bay (~1.0 km/d/de) may also have contributed to the decrease in ice concentration over the ~~NWP~~NOW regime.

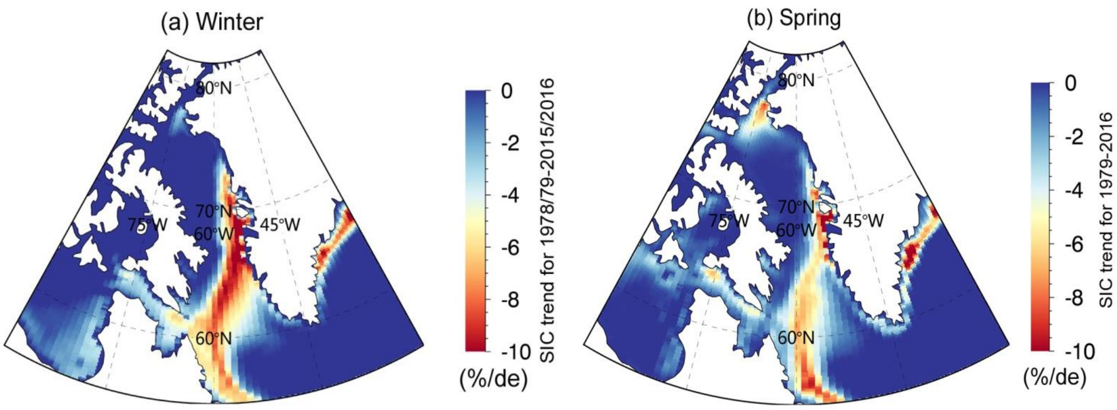

Figure ~~8~~9. Sea ice concentration trends during (a) winter and (b) spring over the period 1978/1979-2016/2017.

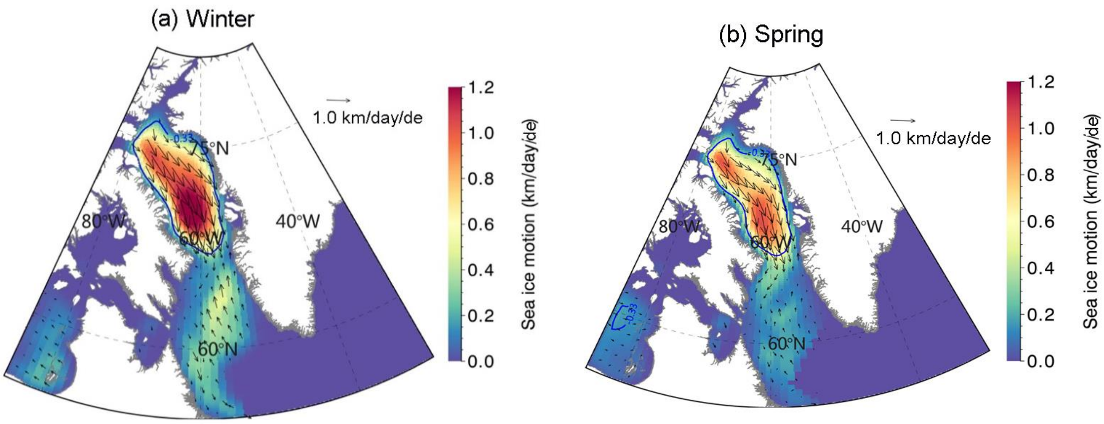

Figure ~~9~~10. As Figure 8 but for sea ice motion fields.

4. Sea ice flux through different fluxgates in Baffin Bay

In this study, sea ice area flux across three gates is obtained. Sea ice inflows to the bay are measured across the North Gate and Lancaster Sound, and the sea ice outflow is estimated across the North Gate (Figure ~~4~~5). The obtained sea ice flow budget (outflow-inflow) provides knowledge of sea ice production or loss associated with the dynamic and thermodynamic processes in the regions between the South and North Gates.

4.1 Monthly variability of sea ice area flux

Figure ~~10~~ 11 shows the monthly mean sea ice area export at the three gates over the period 1978/79-2016/2017. Large monthly variations in sea ice area flux are observed. The average monthly inflow through the North Gate is 17.2×10^3 km^2, with monthly inflow ranging between -0.04×10^3 km^2 (August) and 39.4×10^3 km^2 (January) (Figure ~~10a~~11a). The sea ice flux across the South Gate is greater (Figure ~~10b~~11b). For this gate, the mean monthly export is 32.9×10^3 km^2, nearly twice of that the North Gate, and varies from -0.13×10^3 km^2 (August) to 80.0×10^3 km^2 (January). In comparison, the sea ice area flux across Lancaster Sound is smaller than that of either gate, with an average of 4.6×10^3 km^2 and a range of zero flux (August) to ~10.0×10^3 km^2 (December) (Figure ~~10c~~11c).

The seasonal behaviors of monthly flux for the three gates are similar ~~(Figure 10)~~. In general, the sea ice area flux for the warm period from June to October is low and sometimes reaches to zero. For the cold period from November through next May, it is much larger and varies significantly. Furthermore, there are clear decadal changes as observed for the cold months (November-May). Relative to monthly sea ice flux during the cold months in the first decade (1978-1987), enhanced monthly sea ice flux is observed for the subsequent three decades (since 1988), with average flux values of ~20×10^3 km^2 through the North Gate (Figure ~~8a~~11a), ~50×10^3 km^2 through the South Gate (Figure ~~8b~~11b), and ~5×10^3 km^2 through

Lancaster Sound (Figure ~~8c~~11c). Among the recent three decades, the monthly sea ice flux remains high and does not show significant interdecadal variation.

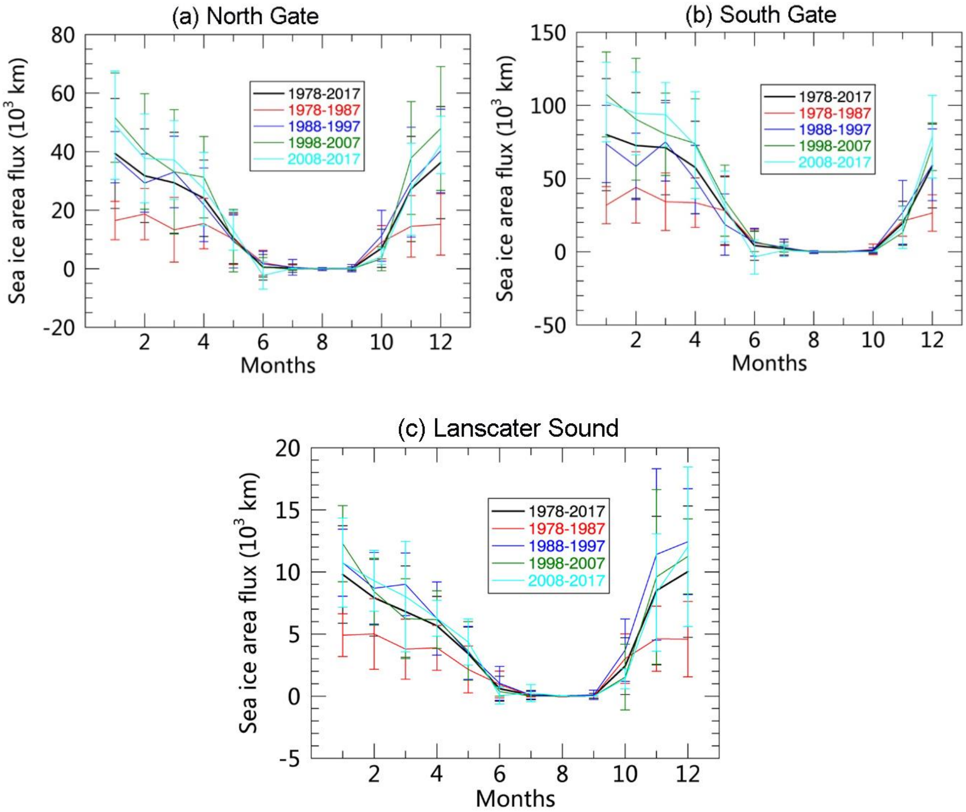

Figure ~~10~~11. Monthly mean sea ice area export in (a) the North Gate, (b) the South Gate, and (c) Lancaster Sound. Both the climatology (1978/1979-2016/2017) and decadal mean fields are given in the panels.

4.2 Variability and trends of seasonal and annual inflow and outflow

Figure ~~11~~ 12 shows the seasonal and annual sea ice area flux across the three gates. The seasonally accumulative flux fields are obtained for the months of spring (March-May), summer (June-~~-~~August), autumn (September-November), winter (December-February). The annual sea ice flux refers to the sum of monthly flux from September to next August.

Distinct interannual variations is evident in the annual sea ice flux fields as well as the winter and spring fluxes (Figure ~~11~~12). Table 2 shows that the average annual inflow across the North Gate is 205.8 ($\pm$74.7)$\times10^3$km^2, with minimum annual inflow in 1980/1981 (64.1$\times10^3$km^2)~~-~~ and maximum annual inflow (414.8$\times10^3$km^2) in 2006/2007. The South Gate shows a mean annual outflow of 394.3 ($\pm$ 110.2) $\times10^3$ km^2, with annual outflow ranging between 140.6 $\times10^3$ km^2 (1980/1981) and 727.4 $\times10^3$ km^2 (2008/2009). The mean annual inflow through Lancaster Sound is 55.2($\pm$17.8)$\times10^3$km^2, with outflow varying between 20.7×10^3 km^2 (1978/1979) and 94.3×10^3 km^2 (2014/2015). The difference between the inflow (through the North Gate and Lancaster Sound) and outflow (through the South Gate), -133.3×10^3 km^2, is suggestive of annual net loss of sea ice area in the regions between ~65 °N and ~75 °N in Baffin Bay.

We obtain a total sea ice inflow of 214.7×10^3 km^2 during the cold seasons (winter and spring) through the North Gate and Lancaster Sound and an outflow of 368.0×10^3 km^2 via the South Gate. The difference of 153.3×10^3 km^2 is largely balanced by newly-formed ice within the bay, revealing the Baffin Bay itself as an important source regime of sea ice. Using ~690×10^3 km^2 as the area of Baffin Bay, this newly formed ice within the bay represents a noteworthy fraction of 22.2% of the coverage of Baffin Bay. As mentioned above, the sea ice motion fields in the bay gradually increase from north to south (Figure ~~7a~~8a), resulting in a distinct ice speed gradient and possibly the occurrence of new leads (not shown). Therefore, the sea ice dynamics of the central and western regions of the bay are dominated by a sea ice diverging pattern (as exemplified in Figure ~~12~~13) where new ice can form from the freezing process in leads. For the warm period (summer and autumn), both sea ice inflow (46.3×10^3 km^2) and outflow (26.3×10^3 km^2) are small. The difference of -20.0×10^3 km^2 represent net sea ice loss that is likely due to enhanced melting in the bay. This finding emphasizes that Baffin bay serves as an important ice sink area during the warm seasons.

Table 2. Seasonal and annual mean sea ice area flux across different gates. (Unit: 10^3 km^2)

Passages	Spring	Summer	Autumn	Winter	Annual
North Gate	63.8	0.63	34.08	107.3	205.8
LS	15.9	0.68	10.9	27.7	55.2
South Gate	156.8	6.2	20.1	211.2	394.3

Note: Spring (March-May); Summer (June-August); Autumn (September-November); Winter (December-February); Annual (September-August).

Figure ~~11~~ 12 shows that all three gates experienced significant positive trends in annual flux over the past four decades, with the major contributions originating from the flux increases during the cold seasons (winter and spring). The trend for the North Gate, approximately 38.9×10^3 km^2/de (or 19.0%/de), is significant (Figure ~~11a~~12a). The percentage trend denotes the fractional change relative to the climatological estimate of flux for 1978/1979-2016/2017. A larger annual increase of 82.2×10^3 km^2/de (or 21.1%/de) is observed for the South Gate (Figure ~~11b~~12b). The increase of ice flux through Lancaster Sound, 7.5×10^3 km^2/de (or 13.6%/de), is small but significant (Figure ~~11c~~12c). All these trend estimates have passed the 99% confidence test. Therefore, the increased sea ice outflow across the South Gate has been partly compensated by the enhanced inflows via the North Gate and Lancaster Sound. The increased outflow across this gate is also partially compensated by the increased occurrence of new ice area formed within the bay.

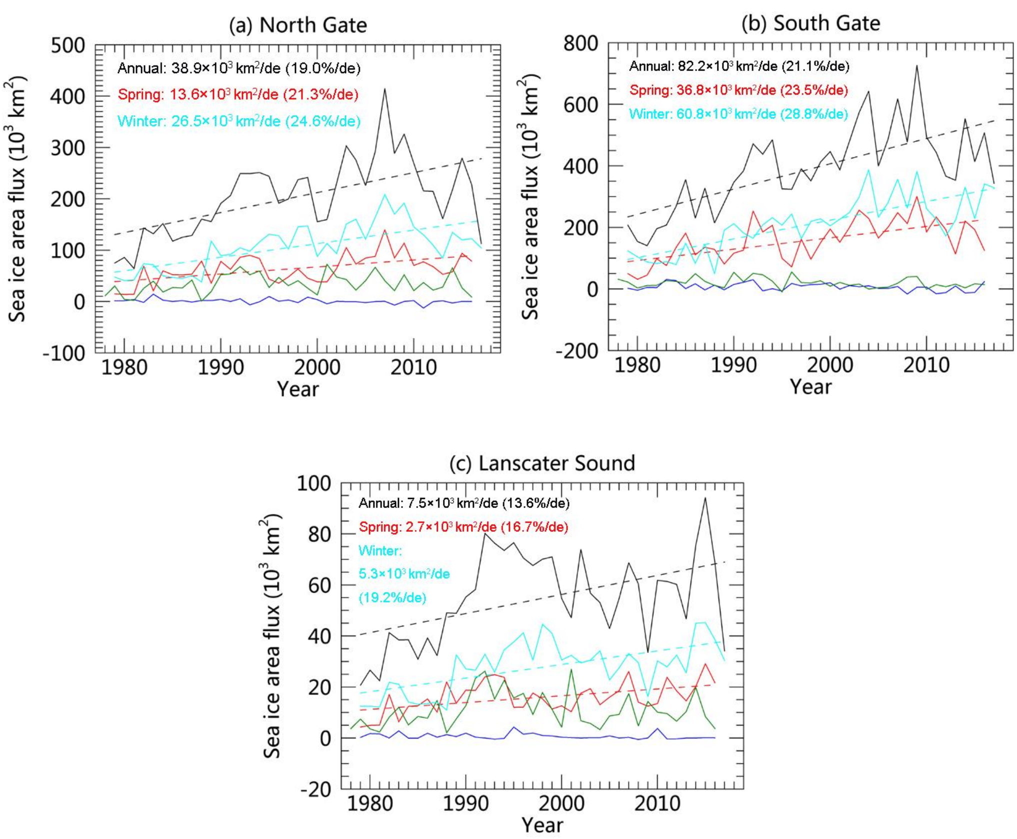

Figure ~~11~~12. Time series of annual (September-August) sea ice area flux (black bold line) across (a) the North Gate, (b) the South Gate, and (c) Lancaster Sound. Seasonal flux is estimated for winter (December – February, cyan line), spring (March-May, red line), summer (June-August, green line), and autumn (September-November, blue line). The dashed lines represent the linearly fitted trends. The annual and cold-season (winter and spring) trends are all significant at the 99% level. However, for the warm seasons (summer and autumn), the trends are not statistically significant and are not shown in the panels.

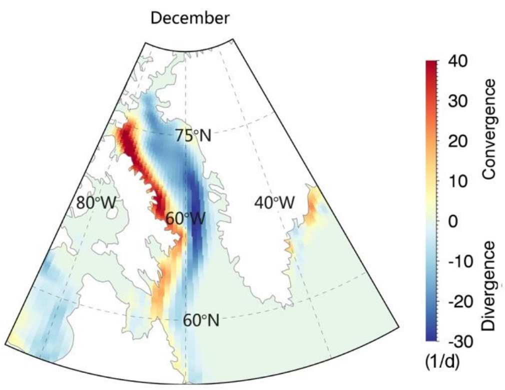

带格式的：字体颜色：文字 1

Figure ~~12~~13. Divergence/convergence fields derived from the climatological (1978/1979-2016/2017) sea ice motion vector fields in December using Equation 3.

5. Discussion

5.1 Possible sources of sea ice inflow into northern Baffin Bay

~~There sources~~The sources that ~~-~~contribute to the ice area changes in northern Baffin Bay, i.e. the area flux through the North Gate, include: (1) inflow from the Arctic Ocean through Nares Strait; (2) inflow from the Canadian Arctic Archipelago (CAA) across Lancaster Sound and Jones Sound (JS); and (3) ice production in ~~NWP~~NOW in the bay;

5.1.1 Nares Strait sea ice inflow through Smith Sound

Sea ice transport in Nares Strait is controlled by the formation of ice bridges in Nares Strait. As reported based on RADARSAT SAR imagery by Kwok (2007), ice bridges form due to increases in the strength of ice arches in the middle to late winter, and collapse due to warm temperatures in early summer. Arching is commonly observed in Kane Basin to the south end of Nares Strait and another occurs in the north end. Over a 13-year period (1997-2009), the South arch formed in all years except 2009, whereas half of the winters lacked the North arch (Kwok, 2007). The formation of the South arch may depend on upstream ice conditions, and the formation of the North arch in the northern inlet of Nares Strait may be favored by the creation of the South arch. The locations of the two ice arches are shown in Figure S1a.

It is clear that when the south arch forms, there exist conditions where sea ice inflow through Nares Strait into the Baffin Bay is strongly restricted under some conditions. Seasonal stoppages of Nares Strait ice flux into Baffin Bay are associated with the formation of the South arch. The immediately mitigating effects due to the formation of ice bridges are apparent from the cases in 2007. During that winter, no locations had conditions suitable for the formation of ice bridges, and area flux through Nares Strait reached to a record high (87×10^3 km^2). This large outflow accounted for 21.0% of the annual ice flux (414.8×10^3 km^2) through the North Gate of Baffin Bay in 2006/2007.

Owing to the small width of Smith Sound (~30 km), the sea ice area flux through Nares Strait cannot be accurately estimated using the coarse NSIDC drift data (25-km resolution) which may be subject to coastal contamination. With high-resolution SAR ice motion data (sampled on a 5-km grid), Kwok (2005) and Kwok et al. (2010) obtained Arctic sea ice inflow through Nares Strait. They estimated an average annual (September-August) ice area flux of 33×10^3 km^2 for a six-year period (1996-2002) and an annual average area flux of 42×10^3 km^2 for a longer, 13-year period (1996-2009). Therefore, sea ice area export via Nares Strait into northern Baffin Bay between 1996/97 and 2008/2009 may contribute a notable fraction (23.3%) of the total ice area flux via the North Gate for the same period (280.2×10^3 km^2).

5.1.2 Sea ice inflow from the Canadian Arctic Archipelago

The sea ice exchange between the CAA and Northern Baffin Bay mainly through Lancaster Sound and the Jones Sound. However, sea ice inflow from the two sounds to the Baffin Bay is difficult to quantify. In an early study for the 1970s, Dey (1981) roughly estimated the average annual inflows of 170×10^3 km^2 and 20×10^3 km^2 for the Lancaster and Jones Sounds, respectively. The sea ice motion fields used were derived from diverse sources, including coarse satellite imagery, airborne observations measurements, as well as field measurements. Therefore, their estimates only correspond to a rough estimate.

In a recent study, Agnew et al. (2008) applied a spatially enhanced AMSR-E sea ice motion (13.5 km) to assess the sea ice area flux across CAA for the period from 2002/2003 to 2006/2007. During the 5-year period, sea ice is exported 68×10^3 km^2 for each year across the Lancaster Sound into Baffin Bay. By contrast, the average sea ice inflow across Jones Sound approaches to zero. In our estimate, the Lancaster Sound sea ice inflow is estimated to be 58.2×10^3 km^2 for the same period, which is comparable to the Agnew's results based on the AMSR-E imagery. Therefore, the Lancaster Sound constitutes one of important ice sources for the sea ice into the Northern Baffin Bay.

5.1.3 Sea ice production in North Water Polynyas

The ~~NWP~~NOW is a distinct feature in northern Baffin Bay. As shown in Figure 6, it usually occupies an area in the north end of Baffin Bay (north of 75 °N) and serves as a large ice production area during freezing periods. As mentioned above, its emergence is largely attributable to the formation of an ice bridge in the south end of Nares Strait (Figure S1a) which controls the sea ice inflow. Maintained by strong northerly winds and ocean currents, this large polynya is frequently exposed, and new sea ice grows within it; this new ice is then transported southward. Based on previously reported CAA inflow through Smith Sound (42×10^3 km^2) and Jones Sound ($0\sim20\times10^3$ km^2), we obtain a preliminary estimate of annual mean area production in the ~~NWP~~NOW ($218\sim238\times10^3$ km^2) for the period 1996/1997-2008/2009. To obtain this estimate, sea ice from the two inflow sources are subtracted from the mean annual ice flux of the North Gate (280.2×10^3 km^2) of the corresponding period. The results suggest the major part (approximately 78~85%) of the sea ice entering via the North Gate is likely produced in the polynya.

5.2 Connections to cross-gate sea level pressure gradient

If free drift conditions are allowed, sea ice motion is mainly wind-driven and parallel to the sea level pressure isobars (Thorndike and Colony, 1982). In this study, the response of daily sea ice flux to the cross-gate pressure gradient was investigated. The gradient is defined as the difference of mean sea level pressure (SLP) between the east and west endpoints of each fluxgate. The positive (negative) gradient corresponds to positive (negative) sea ice flux. The data pairs of SLP gradient difference and ice area flux for each gate are shown in Figure ~~13~~14. Clearly, the cross-gate SLP difference is a good predictor of the variance of sea ice flux for the North (Figure ~~13a~~14a) and South Gates (Figure ~~13b~~14b), with a correlation of

0.62 and 0.68, respectively. These correlations are statistically significant at the 99% confidence level. The stronger slope in the South Gate (0.27) is suggestive of an ice condition that is thinner and perhaps closer to free drift than that of the North Gate (0.23). Lancaster Sound, however, reveals an overall counter gradient ice motion (R = -0.23), although it is not significant (Figure ~~13c~~14c). Sea ice in this narrow channel is largely controlled by internal ice stresses caused by local sea ice interactions and orographic conditions. As a consequence, sea ice floes in the sound can not move as freely as those in the interior part of Baffin Bay.

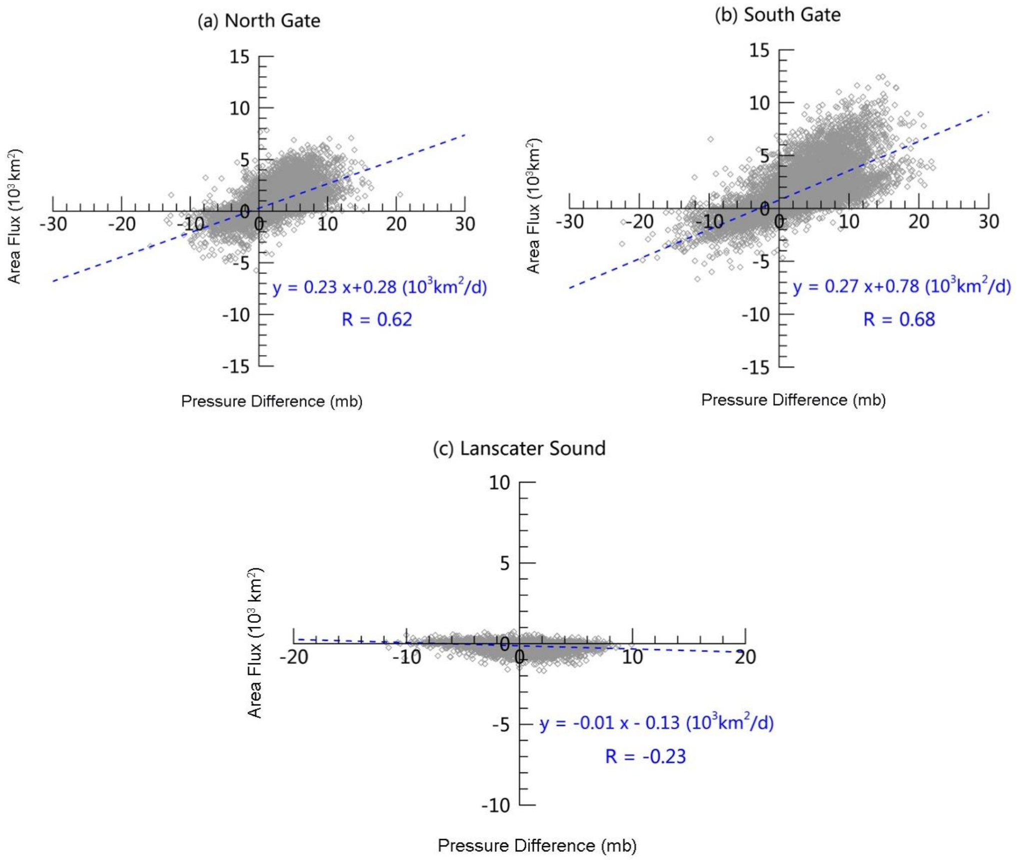

Figure ~~13~~14. Scatterplot of daily sea ice area flux and cross-gate pressure differences for (a) the North Gate, (b) the South Gate, and (c) Lancaster Sound.

5.3 Causes of the enhanced sea ice area flux

5.3.1Potential contribution of geostrophic winds?

According to Equation 1, sea ice motion and concentration are the two essential input parameters to estimate area flux. Potentially, their changes would be reflected in the variations of flux. Figure ~~14~~ 15 depicts the interannual variations and trends of the two relevant sea ice parameters for the cold seasons (winter and summer) at the North and South Gates. As mentioned above and shown in Figure ~~11~~12, all three fluxgates show significant increases in sea ice area flux during the cold seasons. This is mainly caused by the increasing trend in sea ice motion (Figure ~~14~~15). On the other hand, the decreasing trend in sea ice concentration may contributed negatively to ice area flux. The trends are all significant at the 99% level. The increasing or decreasing trends of different parameters at each fluxgate in the context of the entire bay are illustrated in Figures ~~8~~ 9 and ~~9~~10.

Figure ~~14~~ 15 displays the records of cross-gate SLP difference (red bold line), a proxy for the strength of geostropic winds. Although the SLP difference is a good predictor of the interannual variability in ice motion (see section 5.2 for more details), it does not show any significant trend over the nearly 40-yr period. This observation eliminates wind force as a main driver of the positive trends in ice motion and area flux fields.

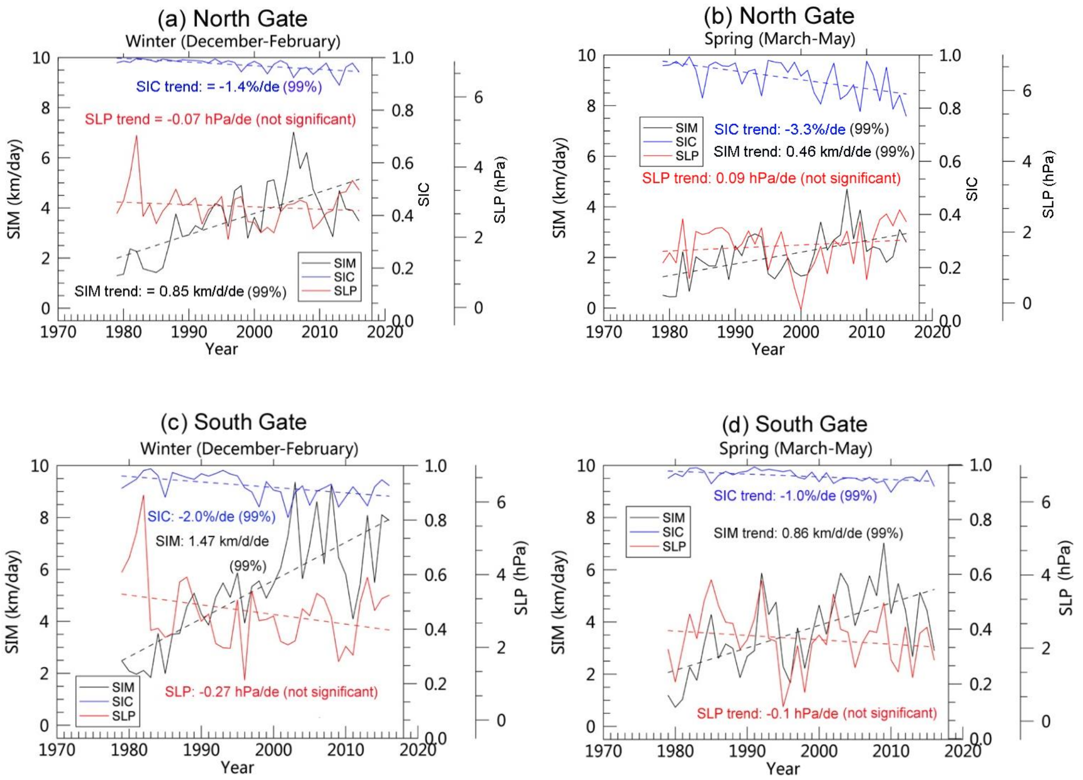

Figure ~~14~~15. Trends and variability of cross-gate mean sea ice motion (black bold line) and concentration (blue bold line) for the (a) North Gate and (b) South Gate. The linear fit line for each parameter is shown as a dashed line. Cross-gate sea level pressure (SLP) difference (red) is shwon to facilitate the analysis of causes of the significant trends in sea ice motion.

5.3.2 Changes in sea ice

Here we examine the changes of sea ice itself, specifically, (1) the changes in sea ice concentration and (2) the changes in sea ice thickness. A reduced sea ice concentration is expected to cause a decreased area flux across the fluxgates. On the other hand, it implies a less compacted ice pack and facilitates sea ice drift and, perhaps, an increase in area flux. Despite the decline in sea ice concentration at each gate during the cold periods, the sea ice generally remains at a compact level above 90% (Figure ~~14~~15), at which large ice internal ice stress is still expected. Therefore, sea ice concentration changes cannot be a primary driver of the enhanced ice motion and area flux.

Due to the scarcity of direct ice thickness measurements, we obtain an approximation of ice thickness changes with time following the Zubov ice growth model. The associated cumulative freezing degree (C_{Fd}) is derived from surface air temperatures~~-~~. This variable is directly related to the level of sea ice growth. Modeled ice thickness fields for different periods are shown in Figure ~~15~~ 16 as a function of ΔC_{Fd}, where ΔC_{Fd} denotes the average daily freezing degree (℃) of the whole growth period. That is, $\Delta C_{Fd} = C_{Fd}/F_d$, where F_d is the total days of an ice growth period.

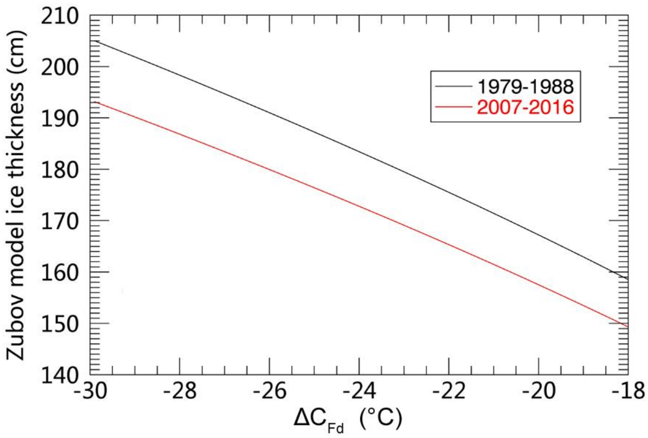

Figure ~~15~~16. Modeled sea ice thickness change as a function of freezing degree (daily average, ΔC_{Fd}) for early (1979-1987) and recent (2007-2016) decades.

The downward slope of each line in Figure ~~15~~ 16 (-3.83 cm/℃ and -3.75 cm/℃ for early and recent decades, respectively) represents the changes in thickness with the freezing air temperature. There is an increasing trend in SAT in the bay of 0.95℃/de (Figure ~~16~~17). Based on estimates displayed in Figure ~~15~~16, this air temperature enhancement implies a SAT increase in the bay of 3.8℃ in the recent decade, which can be expected to cause a thickness decline of 14.6 cm and 14.3 cm (i.e. multiplying slope by 3.8℃) for the early and recent decade, respectively.

The systematic bias between the two lines in Figure ~~15~~ 16 one for each decade, corresponds to the ice thickness change in association with the change in the length of the freezing period. Due to warmer surface air in the recent decade, a difference in ice growth period of approximately 20 days is observed between the two decades (i.e., approximately -5 days/de), which is consistent with the delayed freezing and earlier melting dates in Baffin Bay (Stroeve et al., 2014). When taking into account the freezing period changes, a further ~10 cm decline is identified due to the shortened days of freezing

(Figure ~~10~~11). Therefore, the increased SAT, together with the shortened length of the ice freezing period, can be expected to cause an average reduction in sea ice thickness of 24.6 cm.

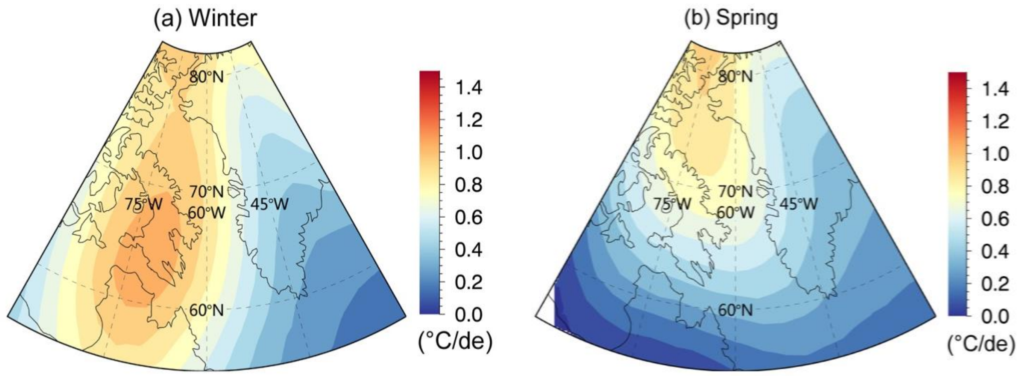

Figure ~~16~~17. Surface air temperature trends for the period 1978/1979-2016/2017 during (a) winter and (b) spring periods

According to Equation (2), sea ice motion acceleration due to air and current dragging force ($\boldsymbol{\tau}_{\mathbf{a}}$ and $\boldsymbol{\tau}_{\mathrm{w}}$) is proportional to the inversion of thickness change (i.e. 1/h). Therefore, the recent ice thickness decline of 24.6 cm for an ice with a typical thickness of 1.8 m would lead to ~~-~~enhanced ice motion, 1.16 times that of the early decade. A recent study indicates that air-ice (water-ice) drag coefficient in Baffin Bay could have a trend of approximately of 0.01 ×10^{-3}/yr (0.06××10^{-3}/yr) (Tsamados et al., 2014). Taking into account these trends, air (water) dragging force would have accelerated the sea ice motion by approximately 1.27 (1.48) times. Together, recent sea ice speed can be enhanced by 1.47~1.72 times now in comparison with that in the earlier period when thicker ice and small drag coefficients prevail.

Although the ice growth model used here is simple, it can reflect the basic trend of a declining ice thickness over past decades. As indicated by the field measurements (Kurtz et al., 2011), recent snow depth over First-year ice in Arctic Ocean seem to be reduced by a half. Another study suggests that decreased snow depth and ice thickness will increase the sea ice thickness growth rate and delay (but not reverse) the sea ice thickness decline trend (https://www.sciencedaily.com/releases/2018/12/181206114700.htm). Therefore, using Equation 2 to estimate sea ice thickness changes without considering the effects of snow changes may overestimate the declining trend of sea ice thickness. However, our estimates suggest ~~Our results prove~~ that winter and spring sea ice motion in Baffin Bay in the recent decade are on average 1.6 times greater than those in the early decade. This is comparable in magnitude to the ice motion changes (our calculations) that are dependent on the changes with respect to decreased thickness and increased drag coefficients ~~changes as we simulated~~. ~~The remaining small part of ice motion acceleration can be explained by ice concentration decline~~. To summarize this section, the sea ice motion and area flux increases in Baffin Bay over the past four decades are mainly attributable to a thinner sea ice thickness which is primarily associated with the increase in surface air temperature. This is consistent with findings in the Arctic Ocean (Rampal et al., 2009; Spreen et al., 2011; Kwok et al., 2013). Also, air and water drag coefficients changes also contributes an significant part to the sea ice motion increases.

带格式的: 缩进：首行缩进： 1 字符

带格式的: 上标

带格式的: 缩进：首行缩进： 2 字符

带格式的: 缩进: 首行缩进: 1 字符

6. Conclusions

. With satellite-derived sea ice parameters, we estimated the sea ice inflow and outflow through the key fluxgates of Baffin Bay. The record of sea ice area flux was extended to span a nearly 40-yr period from 1978/1979-2016/2017. On the basis of the estimates, the variability and trends of sea ice area flux through the three fluxgates (North Gate, Lancaster Sound, and South Gate) for different timescales (monthly, seasonal, and annual flux) are examined in detail. Large interannual variations are detected for the different flux fields. Moreover, significant increasing trends are identified for the annual ice flux for the three gates, with the primary contributions from those during winter (December-February) and spring (March-May).

The spatiotemporal differences are obvious for the sea ice flux through different gates. On average, there is an inflow though North Gate (205.8×10^3 km^2) and Lancaster Sound (55.2×10^3 km^2) and an outflow via South Gate (394.3×10^3 km^2). During cold seasons (winter and spring), the difference between inflow and outflow (i.e. inflow minus outflow) amounts to -153.3×10^3 km^2 and is largely replenished by new ice formed within the bay that is likely associated with the divergence mechanism. For the warm period (summer and autumn), the sea ice inflows (46.3×10^3 km^2) and outflows (26.3×10^3 km^2) are small, pointing to a net ice area loss of 20.0×10^3 km^2 that is connected to melting process in the bay. This emphasizes that the Baffin bay serves as not only an area of ice source during cold periods and but also an area of ice sink during warm periods. The sea ice growth and melting processes could ~~have vital influences~~influence ~~on~~ the ocean current properties in Baffin Bay. With regard to the diverse ice inflow sources into the northern Baffin Bay through the North Gate, the comparisons with published results seem to tally well with the fact that the majority of (about 75%~85%) of ice area originates from ice growth in ~~NWP~~NOW, in addition to the ice inputs via Nares Strait, Lancaster Sound, and Jones Sound.

The interannual variability of ice flux across the North and South Gates is in part linked to wind forcing associated with the cross-gate SLP differences, while the ice flow through Lancaster Sound is largely determined by orographic conditions. The trends for the three gates (North Gate: 38.9×10^3 km^2/de; South Gate: 82.2×10^3 km^2/de; Lancaster Sound: 7.5×10^3 km^2/de) are significant, which are primarily explained by the increasing ice motion and to a small fraction by the decreasing ice concentration. The preliminary simulation demonstrates that the sea ice motion, which has been accelerated over the past four decades, is mainly attributable to the decline in ice thickness and the increase in the air and water drag coefficients in Baffin Bay. Furthermore, modeling results unveiled that the warmer climate plays a decisive role in generating a thinner ice in the bay.

Acknowledgements

The authors would like to thank the data providers as follows. NSIDC provided the satellite-derived ice motion and concentration data, and National Centers for Environmental Prediction/National Center for Atmospheric Research (NCEP/NCAR) provided the reanalysis product. We are grateful for the suggestions from J. Zhang, M. Steel, and A. Schweiger (University of Washington). Also, we appreciate the constructive comments from the three anonymous reviewers. This work was supported by the National Natural Science Foundation of China under Grants 41406215 and 41706194, a fund provided by the Qingdao National Laboratory for Marine Science and Technology, and the NSFC-Shandong Joint Fund for Marine Science Research Centers (U1606401).

References

Aagaard, K., and Carmack, E. C.: The role of sea ice and other fresh water in the Arctic circulation, Journal of Geophysical Research Oceans, 94, 14485–14498, 1989.

Agnew, T., Lambe, A., and Long, D.: 2008: Estimating sea ice area flux across the Canadian Arctic Archipelago using enhanced, Journal of Geophysical Research Oceans, 113, -, 2008.

Bi, H., Huang, H., Fu, M., Fu, T., Zhou, X., and Xu, X.: Estimating sea-ice volume flux out of the Laptev Sea using multiple satellite observations, Polar Research, 35, 2016a.

Bi, H., Sun, K., Zhou, X., Huang, H., and Xu, X.: Arctic Sea Ice Area Export Through the Fram Strait Estimated From Satellite-Based Data:1988–2012, IEEE Journal of Selected Topics in Applied Earth Observations & Remote Sensing, 9, 3144-3157, 2016b.

Cho, K., Sasaki, N., Shimoda, H., Sakata, T., and Nishio, F.: Evaluation and improvement of SSM/I sea ice concentration algorithms for the Sea of Okhotsk, Journal of the Remote Sensing Society of Japan, 16, 47-58, 1996.

Cimatoribus, A. A., Drijfhout, S. S., Toom, M. D., and Dijkstra, H. A.: Sensitivity of the Atlantic meridional overturning circulation to South Atlantic freshwater anomalies, Climate Dynamics, 39, 2291-2306, 2012.

Comiso, J. C., Gersten, R., Stock, L., Turner, J., Perez, G., and Cho, K.: Positive trends in the Antarctic sea ice cover and associated changes in surface temperature, Journal of Climate, 30, 2251–2267, doi:10.1175/JCLI-D-0408.1, 2017a.

Comiso, J. C., Meier, W. N., and Gersten, R.: Variability and trends in the Arctic Sea ice cover: Results from different techniques, Journal of Geophysical Research, 122, 2017b.

Cuny, J., Rhines, P. B., and Kwok, R.: Davis Strait volume, freshwater and heat fluxes, Deep Sea Research Part I Oceanographic Research Papers, 52, 519-542, 2005.

Cuny, J., Rhines, P. B., and Niiler, P. P.: Labrador Sea Boundary Currents and the Fate of the Irminger Sea Water, Journal of Physical Oceanography, 32, 627-647, 2002.

Curry, B., Lee, C. M., Moritz, R. E., and Kwok, R.: Multiyear Volume, Liquid Freshwater, and Sea Ice Transports through Davis Strait, 2004-10, Journal of Physical Oceanography, 44, 1244-1266, 2014.

Dey, B.: Monitoring winter sea ice dynamics in the Canadian Acctic with NOAA-TIR images, Journal of Geophysical Research Oceans, 86, 3223-3235, 1981.

Dunlap, E., and Tang, C. L.: Modelling the mean circulation of Baffin Bay, Atmosphere, 44, 99-109, 2006.

Goosse, H., Fichefet, T., and Campin, J. M.: The effects of the water flow through the Canadian Archipelago in a global ice-ocean model, Geophysical Research Letters, 24, 1507–1510, 1997.

Graham, R. M., Cohen, L., Petty, A. A., Boisvert, L. N., Rinke, A., Hudson, S. R., Nicolaus, M., and Granskog, M. A.: Increasing frequency and duration of Arctic winter warming events, Geophysical Research Letters, 44, 6974-6983, 2017.

Hawkins, E., Smith, R. S., Allison, L. C., Gregory, J. M., Woollings, T. J., Pohlmann, H., and Cuevas, B. D.: Bistability of the Atlantic overturning circulation in a global climate model and links to ocean freshwater transport, Geophysical Research Letters, 38, 415-421, 2011.

Holland, M. M., Bitz, C. M., Eby, M., and Weaver, A. J.: The Role of Ice-Ocean Interactions in the Variability of the North Atlantic Thermohaline Circulation, Journal of Climate, 14, 656-675, 2001.

Jahn, A., Tremblay, B., Mysak, L. A., and Newton, R.: Effect of the large-scale atmospheric circulation on the variability of the Arctic Ocean freshwater export, Climate Dynamics, 34, 201-222, 2010.

Kalnay, E., Kanamitsu, M., Kistler, R., Collins, W., Deaven, D., Gandin, L., Iredell, M., Saha, S., White, G., and Woollen, J.: The NCEP/NCAR 40-Year Reanalysis Project, Bulletin of the American Meteorological Society, 77, 437-472, 1996.

Kurtz N.T, Farrell S.L: Large-scale surveys of snow depth on Arctic sea ice from Operation IceBridge. Geophysical Research Letters, 38, L20505, 2011.

Krumpen, T., Janout, M., Hodges, K. I., and Gerdes, R.: Variability and trends in Laptev Sea ice outflow between 1992–2011, Cryosphere, 7, 349-363, 2013.

Krumpen, T., Gerdes, R., Haas, C., Hendricks, S., Herber, A., Selyuzhenok, V., Smedsrud, L., and Spreen, G.: Recent summer sea ice thickness surveys in Fram Strait and associated ice volume fluxes, Cryosphere, 10, 523-534, 2016.

Kwok R , Curlander J C , Pang S S. An ice-motion tracking system at the Alaska SAR facility. IEEE Journal of Oceanic Engineering, 15, 44-54, 1990.

Kwok, R.: Variability of Nares Strait ice flux, Geophysical Research Letters, 32, 1064-1067, 2005.

Kwok, R., Maslowski, W., and Laxon, S. W.: On large outflows of Arctic sea ice into the Barents Sea, Geophysical Research Letters, 32, 45-81, 2005.

Kwok, R.: Baffin Bay ice drift and export: 2002–2007, Geophysical Research Letters, 34, 2002-2007, 2007.

Kwok, R.: Outflow of Arctic ocean sea ice into the Greenland and Barents Seas: 1979-2007, Journal of Climate, 22, 2438-2457, 2009.

Kwok, R., Toudal, P. L., Gudmsen, P., and Pang, S. S.: Large sea ice outflow into the Nares Strait in 2007, Geophysical Research Letters, 37, 93-101, 2010.

Kwok, R., Spreen, G., and Pang, S.: Arctic sea ice circulation and drift speed: Decadal trends and ocean currents, Journal of Geophysical Research Oceans, 118, 2408-2425, 2013.

Melling, H., Gratton, Y., and Ingram, G.: Ocean circulation within the North Water polynya of Baffin Bay, Atmosphere, 39, 301-325, 2001.

Parkinson, C. L., and Cavalieri, D. J.: A 21 year record of Arctic sea-ice extents and their regional, seasonal and monthly variability and trends, Annals of Glaciology, 34, 441-446, 2017.

Peterson, I. K., and Pettipas, R.: Trends In air temperature and sea ice in the Atlantic Large Aquatic Basin and adjoining areas, Canadian Technical Report, Hydrography, Ocean Science, 290, 2013.

Qian, Y., Dixon, T. H., Myers, P. G., Bonin, J., Chambers, D., and Broeke, M. R. V. D.: Recent increases in Arctic freshwater flux affects Labrador Sea convection and Atlantic overturning circulation, Nature Communications, 7, 10525, 2016.

Rampal, P., Weiss, J., and Marsan, D.: Positive trend in the mean speed and deformation rate of Arctic sea ice, 1979–2007, Journal of Geophysical Research: Oceans, 114~~,~~, 2009.

Rudels, B.: The outflow of polar water through the Arctic Archipelago and the oceanographic conditions in Baffin Bay, Polar Research, 4, 161-180, 2010.

Serreze, M. C., Barrett, A. P., Stroeve, J. C., and Kindig, D. N.: The emergence of surface-based Arctic amplification, Cryosphere Discussions, 3, 11-19, 2009.

Smedsrud, L. H., Sirevaag, A., Kloster, K., Sorteberg, A., and Sandven, S.: Recent wind driven high sea ice area export in the Fram Strait contributes to Arctic sea ice decline, Cryosphere, 5, 821-829, 2011.

带格式的: 正文, 缩进: 左侧: 0 厘米, 首行缩进: 0 厘米

带格式的: 字体颜色: 蓝色

Smedsrud, L. H., Halvorsen, M. H., Stroeve, J. C., Zhang, R., and Kloster, K.: Fram Strait sea ice export variability and September Arctic sea ice extent over the last 80 years, Cryosphere, 11, 65-79, 2017.

Spreen, G., Kern, S., Stammer, D., Forsberg, R., and Haarpaintner, J.: Satellite-based estimates of sea-ice volume flux through Fram Strait, Annals of Glaciology, 44, 321-328(328), 2006.

Spreen, G., Kwok, R., and Menemenlis, D.: Trends in Arctic sea ice drift and role of wind forcing: 1992–2009, Geophysical Research Letters, 38, L19501, 2011.

Stern, H. L., and Heide-Jørgensen, M. P.: Trends and variability of sea ice in Baffin Bay and Davis Strait, 1953–2001, Polar Research, 22, 11-18, 2003.

Stroeve, J., Schroder, D., Tsamados, M., and Feltham, D.: Warm Winter, Thin Ice?, The Cryosphere, 12, 1791-1809, 2018.

Stroeve, J. C., Markus, T., Boisvert, L., Miller, J., and Barrett, A.: Changes in Arctic melt season and implications for sea ice loss, Geophysical Research Letters, 41, 1216-1225, 2014.

Sumata, H., Gerdes, R., Kauker, F., and Karcher, M.: Empirical error functions for monthly mean Arctic sea-ice drift, Journal of Geophysical Research, 120, 7450–7475, 2015.

Tsamados M. , Feltham D. L. , Schroeder D. , et al.: Impact of Variable Atmospheric and Oceanic Form Drag on Simulations of Arctic Sea Ice. Journal of Physical Oceanography, 44, 1329-1353, 2014.

Thorndike, A. S., and Colony, R.:, Sea ice motion in response to geostrophic winds, Journal of Geophysical Research, 87, 5845–5852. 1982.

Tschudi, M., Fowler, C., Maslanik, J., Stewart, J. S., and Meier, W.: Polar Pathfinder Daily 25 km EASE-Grid Sea Ice Motion Vectors.Version 3, NSIDC., Boulder, Colorador, doi:10.5067/O57VAIT2AYYY, [Accessed April, 2016.], 2016.

Yang, Q., Dixon, T. H., Myers, P. G., Bonin, J., Chambers, D., and Mr, V. D. B.: Recent increases in Arctic freshwater flux affects Labrador Sea convection and Atlantic overturning circulation, Nature Communications, 7, 10525, 2016.

Zhang, Z., Bi, H., Huang, H., Liu, Y., and Yan, L.: Arctic sea ice volume export through the Fram Strait from combined satellite and model data: 1979–2012, Acta Oceanologica Sinica, 36, 44-55, 2017.